J. Fluid Mech. (2013), *vol.* 723, *pp.* 587–603.
doi:10.1017/jfm.2013.143

Simulations of turbulent channels with prescribed velocity profiles

Florian Tuerke[1,2],‡ **and Javier Jiménez**[2,3],†

[1]Institut für Strömungsmechanik und Akustik, Technische Universität Berlin, Müller-Breslau-Strasse 8, 10623 Berlin, Germany

[2]School of Aeronautics, Universidad Politécnica de Madrid, 28040 Madrid, Spain

[3]Centre for Turbulence Research, Stanford University, Stanford, CA 94305, USA

(Received 28 June 2012; revised 25 February 2013; accepted 5 March 2013; first published online 16 April 2013)

Direct numerical simulations of turbulent channels with artificially prescribed velocity profiles are discussed, using both natural and purposely incorrect profiles. It is found that turbulence develops correctly when natural profiles are prescribed, but that even slightly incorrect ones modify the Reynolds stresses substantially. That is used to study the dynamics of the energy-containing velocity fluctuations. The stronger (weaker) structures generated by locally stronger (weaker) mean shears have essentially correct isotropy coefficients but they are out of energy equilibrium, with the energy imbalance compensated by turbulent diffusion. The velocity scale in smooth profiles changes with the distance to the wall, and is best described by a friction velocity derived from the local total tangential stress. The behaviour across sharper shear jumps is more consistent with non-equilibrium eddies that relax over wall-normal distances of the order of the distance to the wall, suggesting that the energy equilibrium in the logarithmic layer is not local to a given height, but applies to extended layers homogenized by wall-normal fluxes. Examples of that non-local character are the large-scale inactive fluctuations near the wall, whose velocities do not scale with the local shear stress, but with that of their active 'cores' farther away from the wall.

Key words: turbulent boundary layers, turbulent flows

1. Introduction

This paper discusses direct numerical simulations of turbulent channels in which the instantaneous wall-parallel-averaged velocity is artificially prescribed. The rest of the flow, including all the fluctuations, is computed in the standard manner. For brevity, and since that procedure may be considered the inverse of Reynolds-averaged Navier–Stokes simulations in which the fluctuations are modelled while the mean profile is computed, we will refer to it as 'inverse RANS', or IRANS. Our original motivation, later abandoned, was to shorten the inflow length of direct simulations of turbulent boundary layers (Simens *et al.* 2009) by keeping the mean velocity profile artificially fixed to some empirical approximation over an upstream fraction

† Email address for correspondence: jimenez@torroja.dmt.upm.es

‡ Present address: Laboratorio de Fluidodinámica, Facultad de Ingeniería, Universidad de Buenos Aires, Paseo Colón 850, C1063ACV Buenos Aires, Argentina.

of the simulation box. The idea was to give the turbulent fluctuations some fetch in a 'correct' environment before the flow was fully released, but the experiment failed. The Reynolds stresses became substantially different from their 'natural' values, and, although they returned to their correct levels upon release of the mean profile, the inflow was not shortened.

Irrespective of its merits as a method for generating inflow conditions, the reasons why the Reynolds stresses grew when the profile was kept fixed remained interesting and unclear, and are the subject of this paper. The two possibilities examined by us are that the growth of the fluctuations was due to fixing the mean profile, instead of letting it evolve according to its own equation of motion, or that the fluctuations are sensitive to relatively small deviations of the imposed velocity from its 'correct' shape, and that the approximation used in our tests (Nagib, Chauhan & Monkewitz 2006) was slightly incorrect.

Both results would be interesting, and provide opportunities to explore the dynamics of turbulence. A central problem of wall-bounded turbulence is how the relative intensities of structures of different sizes, associated with different wall distances, adjust themselves so that the mean momentum transfer along the wall-normal direction remains in balance. We will examine two models. Consider first local equilibrium. It is not difficult to construct feedback models in which locally weak structures with insufficient Reynolds stresses result in a local acceleration of the mean velocity, which in turn leads to the enhancement of the velocity gradient and to the strengthening of the local fluctuations. It is conceivable that fixing the mean profile disrupts that mechanism.

For example, consider a open channel between a no-slip wall at $y = 0$, where the tangential stress is $\tau_w = 1$, and a free-slip surface at $y = 1$. The wall-parallel-averaged momentum equation can be written as,

$$\partial_t S = \partial_{yy} \tau, \tag{1.1}$$

where S is the mean shear and τ is the total tangential stress. Equilibrium requires that $\tau = 1 - y$, but the stability of small perturbations about that state depends on the relation between τ and S. In the simplest assumption that $\tau = \tau(S)$, the equation for stress fluctuations, $\widetilde{\tau}$, is

$$\partial_t \widetilde{\tau} = (\mathrm{d}\tau/\mathrm{d}S)\, \partial_{yy} \widetilde{\tau}, \tag{1.2}$$

and stability requires that $(\mathrm{d}\tau/\mathrm{d}S) \geqslant 0$ everywhere. The experiments in this paper can be understood as a way of exploring the relation between the total stress and the velocity profile by perturbing the latter. In general, they involve modifying the equations of motion, but, as stressed in previous works, that is one of the strengths of numerical simulations (Jiménez & Pinelli 1999).

A second model, not necessarily inconsistent with the first one, is that the momentum balance is a property of the correct mean velocity profile as a whole. The classical theory, as represented by the logarithmic-layer argument of Townsend (1976), is that the turbulent energy production, which is proportional to the mean shear and to the tangential Reynolds stress, balances the local dissipation, which is proportional to the cube of the fluctuation intensities. That would explain why changing the mean profile, and therefore the production, modifies the intensities, but it would also suggest that the latter are determined by the local mean shear, with an interesting lack of interaction among structures at different wall distances. The present experiments would then be useful in differentiating between local and global contributions to the equilibrium of energy and momentum, by allowing us to consider

profiles that differ from the canonical one in different ways at different distances from the wall. In fact, one of the results of this paper will be that energy equilibrium of the Reynolds-stress-bearing scales has to be understood in terms of production and dissipation integrated over 'attached' layers extending to the wall, in agreement with the models of Townsend (1961), Perry & Abell (1975) or Perry, Henbest & Chong (1986), rather than holding at individual wall distances. It will also turn out that the near-wall 'inactive' motions, which carry energy but no tangential stress, derive their velocity scales from their detached 'active' parts, also in agreement with Townsend (1961) model.

Effects similar to those discussed here had been observed by P. Moin (private communication) and Jarrin (2007), associated in both cases with attempts to shorten the initial transient in large-eddy simulations of channels, but they were not analysed in detail. A distant precursor can also be found in the 'constrained Euler' simulations of isotropic turbulence with prescribed spectra, used to study the energy transfer and the behaviour of large-eddy simulations by Shtilman & Chasnov (1992), Jiménez (1993), She & Jackson (1993) and Zhou (1993), among others.

The organization of the paper is as follows. The numerical experiments are described in § 2, followed in § 3 by the presentation and discussion of the results, and by conclusions in § 4. Additional details can be found in earlier reports by Jiménez (2010) and Tuerke (2011).

2. The numerical experiments

The simulations are performed in doubly periodic computational channels with a half-height h, and streamwise and spanwise periodicities $2\pi h$ and πh, as in Moser, Kim & Mansour (1999). It was shown by del Álamo *et al.* (2004) that even smaller boxes have little effect on the spectral energy distribution of the resolved scales, and that scales longer or wider than the box, which are represented in the simulations by wavevectors with zero streamwise or spanwise wavenumbers, carry the correct Reynolds stresses. Flores & Jiménez (2010) showed later that the mean and fluctuating velocities of channel turbulence remain normal up to a wall distance approximately one-third of the spanwise periodicity, which would include the whole present channels. We will concern ourselves with the behaviour of the flow above the viscous layer, and, as a safeguard against possible effects of the box size, mostly centre on the region below $y/h \approx 0.6$. We use u, v and w for the streamwise, wall-normal and spanwise components of the velocity vector $\boldsymbol{u}$, and x, y and z for the respective spatial coordinates. Capital and primed symbols respectively represent mean and root-mean-squared quantities with respect to the average $\langle\ \rangle$, defined over the two homogeneous directions and time. Instantaneous wall-parallel averages, which are equivalent to the $(0,0)$ modes of the two-dimensional (x,z) Fourier expansions of the corresponding quantities, are denoted, for example, by $\widehat{u}_{00}$. The '+' superscript refers to quantities normalized with the friction velocity u_τ and with the kinematic viscosity ν. Density is assumed unity and dropped from the equations. Most of the simulations in this paper have friction Reynolds numbers $h^+ \approx 950$. A second set of simulations was run at $h^+ \approx 550$, with similar results. They are not emphasized, because of their limited scale separation. but they are occasionally used to differentiate between inner and outer length scalings.

Note that even if the Reynolds number is marginal from the point of view of scale separation, the range between $y^+ \approx 100$ and $y/h \approx 0.5\,(y^+ \approx 500)$ can be considered as relatively free from both viscous and outer effects. We will loosely refer to that

range as 'logarithmic', in the spectral sense that the wavelength of the peak of the premultiplied velocity spectrum grows linearly with y (see, for example, figure 1 in Jiménez 2012). A more conservative definition of the logarithmic layer, in terms of the mean velocity profile, only extends to $y/h \approx 0.15$, especially in boundary layers (Nagib *et al.* 2006), but that outer limit is mostly due to the relatively strong 'wake' component of the mean velocity profile in external flows, which is a consequence of the rotational–irrotational intermittency along the edge of the boundary layer (Jiménez & Hoyas 2008). The wake is much weaker in internal flows, and it was shown by Mizuno & Jiménez (2011) that the logarithmic fit of the mean profile can be extended in channels to $y/h \approx 0.5$ by a simple modification of the classical law. Moreover, neither the logarithmic mean profile nor the linear spectral scaling will be particularly important in most of the following. We will basically only require that viscous effects be negligible ($y^+ \gg 100$), which is easily satisfied for most of the $h^+ = 950$ simulations.

The numerical code integrates the incompressible Navier–Stokes equations for the wall-normal vorticity and for the Laplacian of the wall-normal velocity, as in Kim, Moin & Moser (1987), with the mass flux kept constant. The spatial discretization is dealiased Fourier in the homogeneous wall-parallel directions, and Chebychev in the wall-normal one, using $768 \times 385 \times 768$ collocation points along x, y and z. The collocation resolution is $\Delta_x^+ = 7.8$, $\Delta_z^+ = 3.9$ and $\Delta_y^+ = 0.03$–7.7, and time advancement is third-order semi-implicit Runge–Kutta (Spalart, Moser & Rogers 1991). The simulations were run for 10 eddy-turnover times, h/u_τ, and statistics were accumulated over the last $6h/u_\tau$. The initial condition for all the simulations was the same statistically converged field of a standard simulation at the same h^+.

In all but the reference numerical experiments, or in the case F92 discussed below, the evolution equations for the $(0, 0)$ Fourier modes of the three velocity components are substituted by fixed prescribed mean profiles. Their evolution equation, e.g. $\partial_t \widehat{u}_{00} = \widehat{N}_{x,00}$, where $\widehat{\boldsymbol{N}}_{00}$ is the wall-parallel-averaged right-hand side of the Navier–Stokes equation, is therefore substituted by

$$\partial_t \widehat{u}_{00} = \partial_y \widehat{\tau}_{x,00} - \widehat{\partial_x p}_{00} + f_x = \widehat{N}_{x,00} + f_x, \tag{2.1}$$

where $\tau_x = \nu \partial_y u - uv$ is the total streamwise shear stress. Requiring

$$\partial_t \widehat{u}_{00} = 0, \tag{2.2}$$

defines a body force per unit mass,

$$f_x = \widehat{f}_{x,00} = -\widehat{N}_{x,00}, \tag{2.3}$$

that depends only on y and on time. Since the net effect of (2.3) is to enforce (2.2), and therefore to keep $\widehat{u}_{00}$ identical to its initial condition, (2.1) is implemented in the code by prescribing $\widehat{u}_{00}$ at each time step, using (2.3) to compute f_x. The spanwise component is similarly set to $\widehat{w}_{00}(y, t) = 0$, while $\widehat{v}_{00}(y, t)$ vanishes from continuity. Note that the only direct effect of $\widehat{u}_{00}$ on the stress $\widehat{N}_{x,00}$ is through the viscous term $\nu \partial_{yy} \widehat{u}_{00}$, which is negligible above the buffer layer. Its direct contribution to the Reynolds stress, $\langle \widehat{u}_{00} v \rangle = \langle \widehat{u}_{00} \widehat{v}_{00} \rangle$, vanishes identically. The force in (2.3) is only defined up to a constant, which can be absorbed into the mean pressure gradient, $\widehat{\partial_x p}_{00}$, which is adjusted every time step to maintain a constant mass flux. From now on, we

	Symbol	β	y_b/h	h^+	U_bh/ν	Prescribed
C90	–△–	0	N/A	934	18518	Profile
C91	——	+0.5	N/A	950	20012	Profile
C92	– – –	−1	N/A	950	17654	Profile
F92	- ○ - -	−1	N/A	950	17654	Force
B9L	–▼–	−1	0.25	931	18518	Profile

TABLE 1. Parameters of the IRANS profiles. The mixing parameter β is defined in (2.5), and y_b is the centre of the blending layer.

will assume that

$$\int_0^{2h} f_x \,\mathrm{d}y = 0. \tag{2.4}$$

In the simplest IRANS case C90, the streamwise mean velocity is fixed to the long-term average, $U_n(y)$, of a standard simulation in a similar computational box, which is assumed to be 'correct', and that will be denoted from now on as 'natural'. It agrees with the larger channel at the same Reynolds number by del Álamo *et al.* (2004).

The IRANS experiments, C91 and C92, summarized in the upper part of table 1, use a mixed mean profile

$$\widehat{u}_{00} = U(y;\beta) = (1-\beta)U_n(y) + \beta U_C(y), \tag{2.5}$$

where U_C is the profile obtained by integrating $\partial_y U_C = u_\tau^2(1-Y)/\nu_t$, where $Y = y/h$, and the total viscosity,

$$\frac{\nu_t}{\nu} = \frac{1}{2} + \frac{1}{2}\left\{1 + \frac{\kappa'^2 h^{+2}}{9}\left[2Y - Y^2\right]^2\left[3 - 4Y + 2Y^2\right]^2\left[1 - \exp\left(\frac{-y^+}{A}\right)\right]^2\right\}^{1/2}, \tag{2.6}$$

depends on κ' and A (Cess 1958). The best fit to the natural profile at $h^+ = 950$ is $\kappa' = 0.438$ and $A = 27.76$, but the IRANS mean profiles are constructed using (2.5)–(2.6) with the 'unnatural' values $A = 51.5$ and $\kappa' = 0.5$, which tend to increase the shear near the wall if $\beta > 0$, and near the centreline if $\beta < 0$. The friction velocity and the molecular viscosity are adjusted to fix h^+, and to keep the same mass flux as the natural simulations.

A second set of profiles was constructed from C90 and C92, blending $\beta = 0$ near the wall to $\beta = -1$ away from it, using a cubic spline in $|y - y_b| \leqslant 0.075h$, continuous and with continuous first derivatives at its two end points (see figure 1). The profiles were later made symmetric with respect to the channel centreline. Three blending locations were used to represent the buffer, logarithmic, and outer layers, but only the 'logarithmic' blend B9L is discussed here ($y_b = 0.25h$, see table 1). The viscosity and mass flux of these simulations are kept the same as in the natural one, which requires rescaling u_τ and h^+ slightly.

The mean velocity and shear profiles for the IRANS simulations are shown in figure 1. The wall-scaled profiles in figure 1(*a*) differ appreciably from each other, mostly because u_τ is changed by (2.5), but figure 1(*b*), where the velocities are normalized with the natural profile, shows that the difference is never more than 5%. Note the closer agreement in figure 1(*a*) of C90 and B9L, which share the same wall shear; the slight mismatch in figure 1(*b*) between the inner parts of C90 and B9L is due to the rescaling of the friction velocity mentioned at the end of the previous

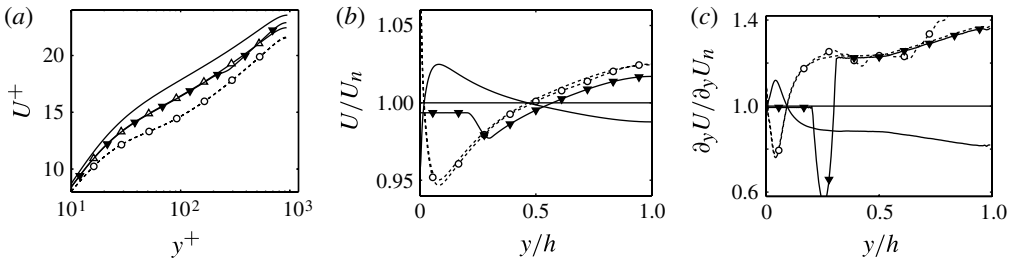

FIGURE 1. Prescribed profiles for the IRANS simulations. (*a*) Mean velocity in wall units. (*b*) Velocity and (*c*) shear, normalized with the unconstrained profiles. Symbols as in table 1.

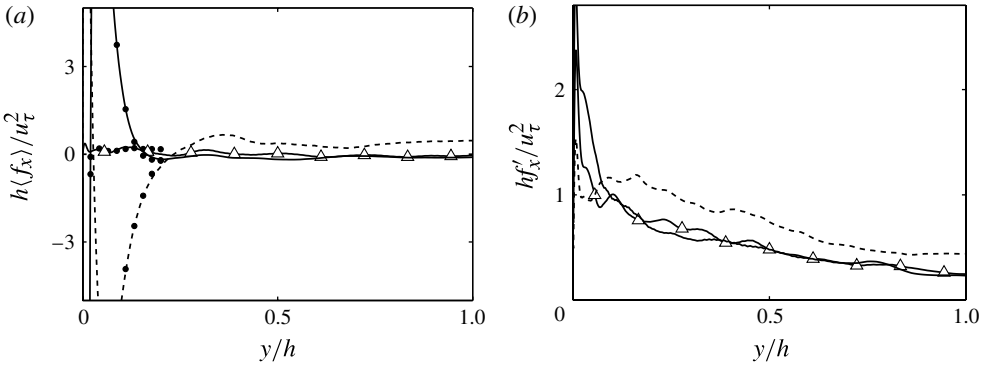

FIGURE 2. (*a*) Average body force $\langle f_x\rangle$, obtained from (2.3). The solid dots are obtained from the overall momentum balance in (3.3), as a test for the statistical equilibrium of the simulation. (*b*) Root-mean-squared body force fluctuations. Symbols for C90–C92 are as in table 1.

paragraph, but is difficult to appreciate in either figures 1(*a*) or 1(*c*) because their vertical scales are respectively 100 and 10 wider than in figure 1(*b*). Figure 1(*c*) shows that the shear $\partial_y U$ varies more than the velocity, $\sim$20 %, although the changes are still an order of magnitude weaker than the natural vorticity fluctuations, which can be estimated from the energy dissipation to be $|\omega'| \approx (\kappa y^+)^{1/2}\,\partial_y U$, where κ is the Kármán constant, and are therefore at least 4–6 stronger than $\partial_y U$ above the buffer layer.

Figure 2(*a*) presents the time-averaged IRANS force, $F_x = \langle f_x\rangle$, obtained from (2.3). Comparing figures 1(*c*) and 2(*a*) suggests that F_x is more closely related to the difference between the natural and prescribed mean shears, which intersect one another near $Y = 0.1$, than to the mean velocities, which intersect near $Y = 0.5$. That was confirmed by testing a case whose shear intersects the natural one at a different location from the ones above. The sign of the force tracks approximately the excess in shear with respect to the natural profile. We will briefly return to this point when discussing figure 4.

3. Results

The first interesting result is that fixing the mean velocity profile to its natural value, as in case C90, does not change the intensity of the fluctuations, showing that a

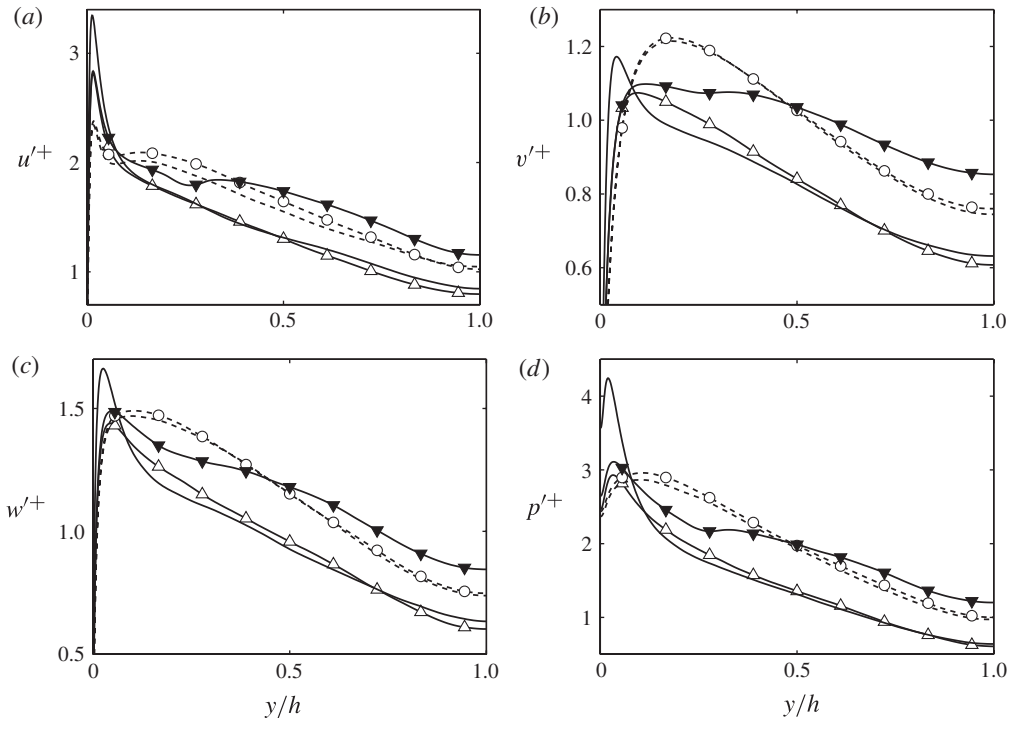

FIGURE 3. (*a*) Streamwise, (*b*) wall-normal, and (*c*) spanwise velocity, and (*d*) pressure fluctuation intensities, for the simulations in table 1. Symbols as in the table.

feedback cycle between the mean profile and the fluctuations, such as the one in the example (1.1), is not required for the stability of the flow, and that any effect of the fluctuations on the mean profile can be replaced by a hard prescription. Note that this is not a trivial result. Figure 2(*a*) shows that the mean IRANS force vanishes in C90, but its instantaneous value does not. Figure 2(*b*) shows that the root-mean-squared temporal fluctuations of the force, f_x', are of the same order as the driving pressure gradient u_τ^2/h over most of the channel, and substantially higher near the wall.

On the other hand, the velocity fluctuation intensities are very sensitive to minor variations of the mean profile. Figure 3 shows intensity profiles for the IRANS simulations. The 'flat' case C91, which has a stronger shear near the wall than the natural one, has stronger intensities in the buffer layer and slightly weaker ones above it. The 'round' profile C92 which has a stronger shear in the central part of the channel and a milder one near the wall, shows the opposite trend, and the same is true for the pressure fluctuations in figure 3(*d*).

Figure 3 also includes the blended profile B9L, which will be discussed later, and case F92, which was run by adding to the right-hand side of (2.1) a constant volumetric force equal to the mean F_x computed for C92, instead of fixing the mean velocity. That simulation is also included among the mean profiles of figure 1(*a*) and there, as well as in figure 3, the results are close enough to C92 for the lines to overlap and to be hard to distinguish visually. The prescribed-force simulation has also been added to figure 1(*b*,*c*), where the differences are more visible, suggesting a slightly stronger wake component in F92 than in C92. However, note again the

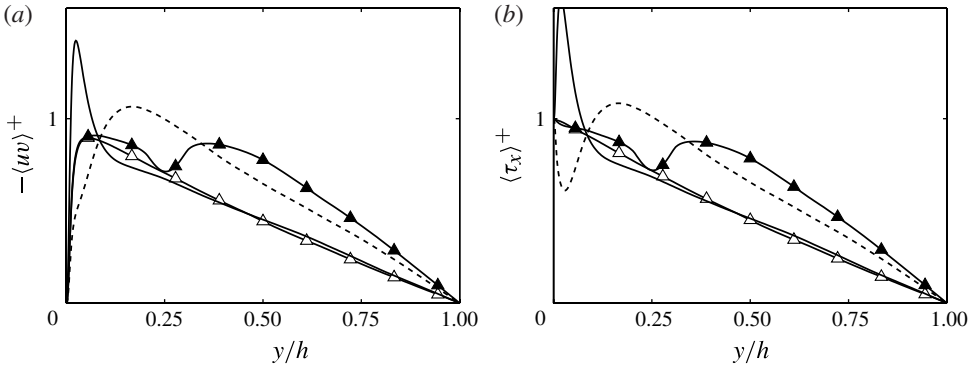

FIGURE 4. (*a*) Tangential Reynolds stress. (*b*) Total stress. Symbols as in table 1.

different vertical scales of figure 1(*a–c*). The similarity between fixing the force and the velocity is consistent with the previous observation that fixing the natural IRANS profile, which involves a force with zero average and large temporal fluctuations, gives similar results to the unconstrained simulations, in which the forcing is kept fixed to the same (zero) average.

Those results suggest that the forcing acts mostly through the effect of the mean profile on the fluctuations, rather than by injecting energy directly into them. That this is the case can be shown from the equation for the fluctuating kinetic energy,

$$\partial_t \langle |\boldsymbol{u}|^2\rangle/2 - \langle \boldsymbol{u}\cdot\boldsymbol{N}\rangle = \langle \boldsymbol{u}\cdot\boldsymbol{f}\rangle. \tag{3.1}$$

The right-hand side is the energy injected by the IRANS force directly into the fluctuations. It vanishes identically because $\boldsymbol{f}$ is spatially uniform over wall-parallel planes. It only has a $(0,0)$ Fourier mode, and is instantaneously orthogonal under spatial averaging to all but the $(0,0)$ Fourier component of the velocity, so that

$$\langle \boldsymbol{u}\cdot\boldsymbol{f}\rangle = \langle \widehat{\boldsymbol{u}}_{00}\cdot\boldsymbol{f}\rangle. \tag{3.2}$$

The average in the right-hand side of this equation involves only time, but, in each of the two types of simulations mentioned above, constant-velocity or constant-force, one of the two factors is constant in time, and can be taken out of the average, while the other one has zero mean. The direct effect of the force on the fluctuating energy therefore vanishes.

Figure 4(*a*) shows that the tangential Reynolds stresses, $-\langle uv\rangle$, of the IRANS simulations differ significantly from one another, and figure 4(*b*) shows that those differences are not compensated by the viscous stress. In natural simulations, the gradient of the total stress $\langle \tau_x\rangle = u_\tau^2(1-Y)$ balances the mean pressure gradient (Townsend 1976, p. 133), and it follows from (2.1) that the deviation of the observed $\langle \tau_x\rangle$ from that linear law is due to the averaged IRANS force. Averaging (2.1) over time, integrating over y to eliminate the mean pressure gradient, and using the normalizing condition (2.4), one obtains

$$h\langle f_x\rangle/u_\tau^2 = -1 - \partial_Y\langle \tau_x^+\rangle, \tag{3.3}$$

which can be used as a check on the average force computed directly from (2.3). The results are included as heavy dots in figure 2(*a*). Note that, after integrating (3.3), figure 4(*b*) can be interpreted as the total force exerted over a layer extending from

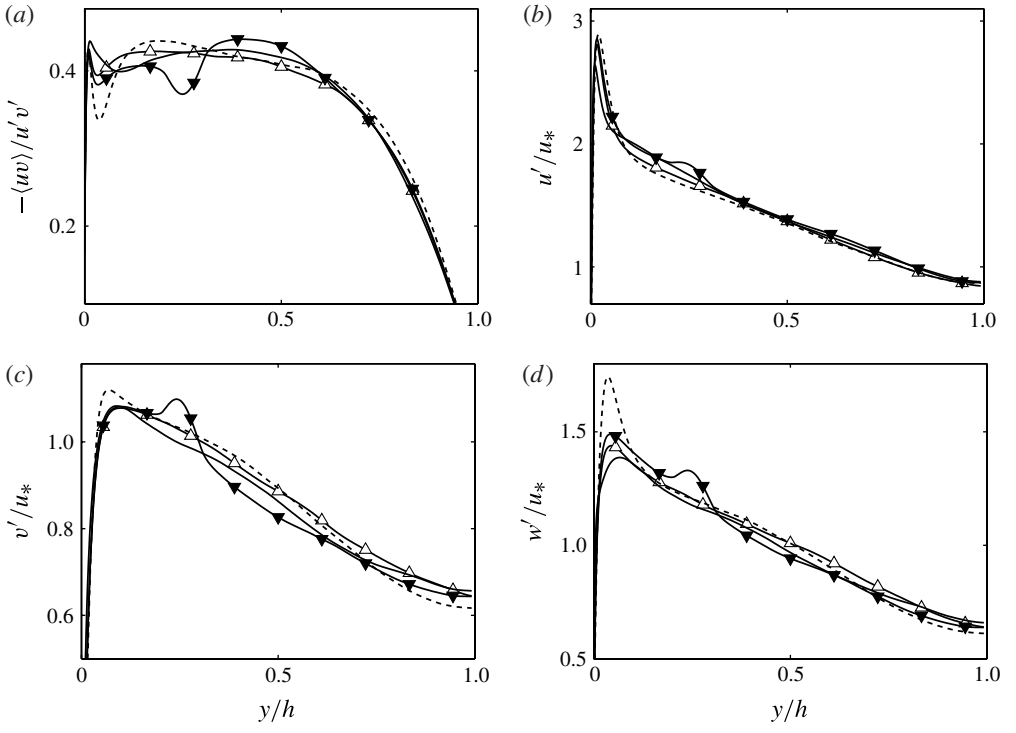

FIGURE 5. (*a*) Stress correlation coefficient, $-\langle uv\rangle/u'v'$. (*b*) Streamwise, (*c*) wall-normal, and (*d*) spanwise velocity fluctuation intensities, normalized with the local friction velocity (3.4). Symbols as in table 1.

the wall to a given distance, and therefore as the contribution of the forcing to the momentum flux τ_x. Comparing it with figure 1 shows even more clearly than figure 2 that the IRANS force follows the mean shear, rather than the velocity.

3.1. *Active and inactive motions*

Figure 5(*a*) reveals that, even with the differences just discussed, the correlation coefficient of the fluctuations, $c_{uv} = -\langle uv\rangle/u'v'$, is very similar for all the cases, including the natural one, especially above the buffer layer. Since c_{uv} can be interpreted as a measure of the efficiency of the turbulent eddies in transporting momentum, this suggests that the structure of the Reynolds-stress-bearing eddies in the IRANS channels, or at least the way that they transfer momentum, is not very different from those in natural ones. It also suggests that the fluctuation profiles of the different simulations should collapse better when normalized with a 'local' friction velocity defined as

$$u_*(Y) = [\langle\tau_x\rangle/(1-Y)]^{1/2}, \tag{3.4}$$

which takes into account the stresses introduced by the IRANS force, instead of with a single u_τ. That is confirmed by figure 5(*b–d*), which includes flat and rounded IRANS profiles, as well as the blended case B9L, whose stresses have an almost discontinuous jump near $y = 0.25h$. Some non-equilibrium effects visible in figure 5 within and above the blending layer of B9L will be analysed in more detail in the next section,

but, even in that extreme case, the collapse is much better than the classical scaling in figure 3.

It is interesting that the collapse with the local stress degrades near the wall for the wall-parallel intensities and for c_{uv}. That behaviour is consistent with the influence of the 'inactive' motions proposed by Townsend (1961), who noted that the intensities of the wall-parallel velocity components do not need to decay as they approach the wall, except within the viscous layer, but that v and the tangential Reynolds stress are blocked by the impermeability condition. Therefore, flow structures with wall-parallel dimensions $O(\lambda)$ would be inactive from the point of view of momentum transfer below some $y \sim O(\lambda)$, carrying energy but no tangential stress. Townsend (1961) also proposed that structures that are inactive near the wall are maintained by Reynolds stresses further up, so that inactive motions are the 'roots' of detached active structures. Spectra of an attached (u) and a detached ($-uv$) variable are represented in figure 6(*a*,*b*) as context for the discussion below. The attached spectrum E_{uu} extends all the way to the wall, even for the longest scales of the large computational boxes, $L_x = 8\pi h$, in figure 6(*a*), but E_{uv} is restricted to wavelengths $\lambda \sim y$, leaving an inactive 'wedge' of long structures near the wall (Perry & Abell 1975; Perry *et al.* 1986). A recent compilation of similar data over a wide range of Reynolds numbers can be found in Jiménez & Hoyas (2008).

The classical theory (Townsend 1976, pp. 135–139) for the scaling of the velocity fluctuations with u_τ is that they have to carry the tangential stresses, $\tau \approx u_\tau^2 \approx -\langle uv \rangle \sim u'^2$. That argument would not seem to apply to inactive structures, but is restored if those structures are the roots of detached active ones, and inherit their scaling from them. The progressive accumulation near the wall of increasingly long and wide inactive scales as the Reynolds number increases, each of them with intensities proportional to u_τ^2, is behind the well-known observations of logarithmic intensity profiles of attached velocity fluctuations, (Townsend 1961; Jiménez & Hoyas 2008; Hultmark *et al.* 2012) of the logarithmic growth of the near-wall maximum of u'^{2+} (deGraaff & Eaton 2000; Metzger & Klewicki 2001; Hoyas & Jiménez 2006), and of the k^{-1} spectrum of the streamwise velocity (Perry & Abell 1975; Perry *et al.* 1986; Perry & Li 1990). Recent reviews are Smits, MacKeon & Marusic (2011) and Jiménez (2012).

In natural flows, it is difficult to distinguish between active and inactive motions from their intensities because, as we have just seen, they share the same velocity scale, but the fluctuations in IRANS simulations scale differently near and far from the wall, and active motions, whose scale is determined locally, can be easily separated from inactive ones, whose velocity scales are determined by their remote active cores. That is seen in figure 6(*c*), which is an enlargement of the near-wall region of figure 5(*a*), with added cases at different Reynolds numbers. All the correlation coefficients c_{uv} have minima below $y^+ \approx 100$, where u' does not scale well with the tangential stress, partly because viscosity carries some of the total stress, but mainly because of the inactive component just discussed. The minima of the two IRANS cases, both of which correspond to 'rounded' profiles with stronger outer fluctuations, are deeper than in the natural cases, and it is tempting to interpret that observation as evidence that the inactive components of those cases scale with their stronger outer u_* instead of with the local ones. That the effect is confined to the inactive wedge of wavelengths is confirmed by figure 6(*d*), which presents the difference between the streamwise spectra $E_{uu}(\lambda_x, y)$ of the IRANS simulation C92 and the natural one C90. Both are normalized with their local u_*, which works well in the active core that includes most

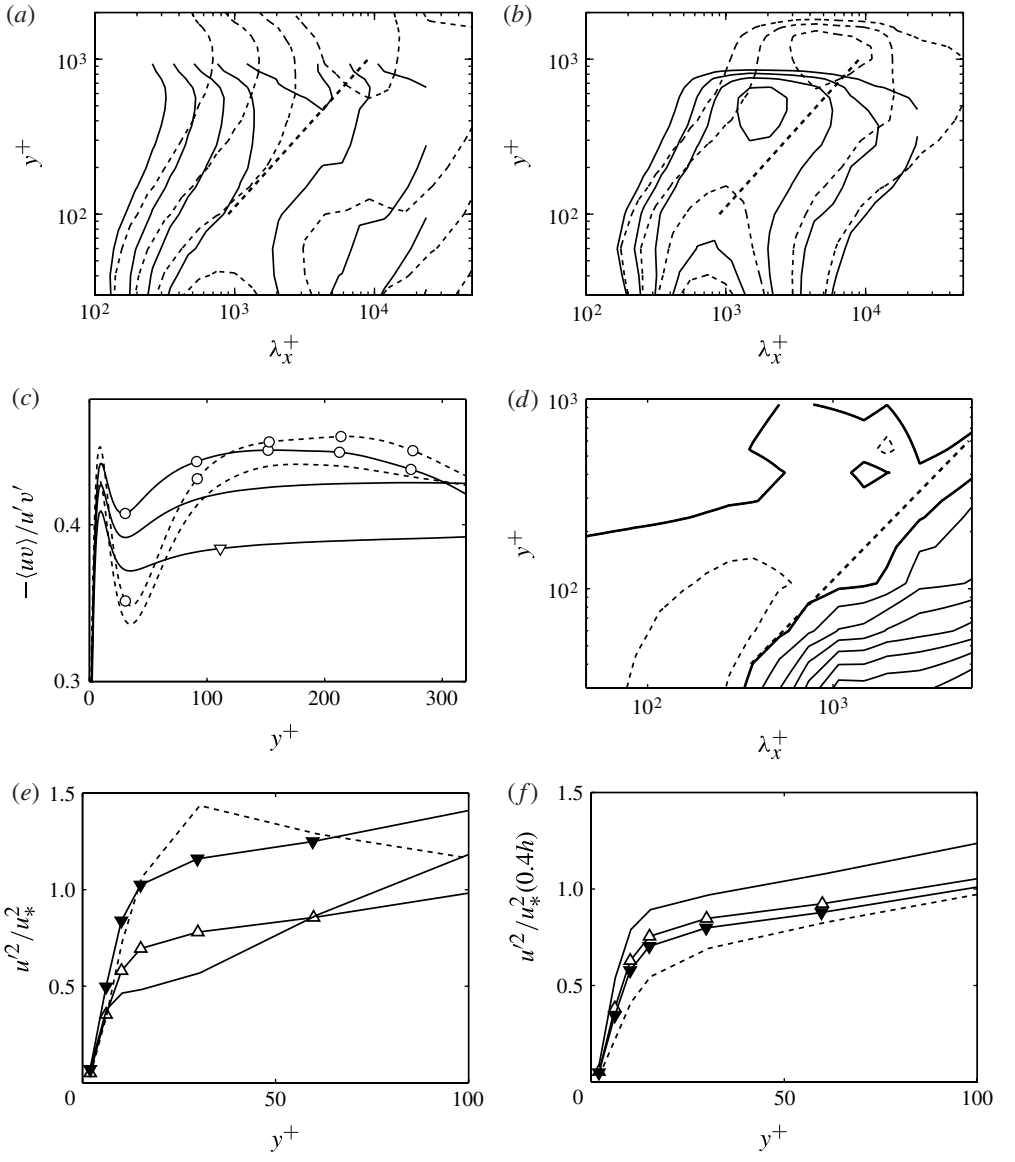

FIGURE 6. (*a*) Normalized premultiplied spectrum, $k_x E_{uu}/u'^2$ of natural channels, against the streamwise wavelength. Wall scaling. Contours are 0.08(0.04)0.2. ——, $h^+ = 934$ (del Álamo *et al.* 2004); – – –, $h^+ = 2003$ (Hoyas & Jiménez 2006). (*b*) Same as (*a*) but for $-k_x E_{uv}/u'v'$. Contours are 0.05(0.02)0.11. (*c*) Stress correlation coefficient, $-\langle uv\rangle/u'v'$. ——, Natural channels; – – –, IRANS with $\beta = -1$. Lines with circles are $h^+ = 550$ and those without are $h^+ \approx 950$. –▽– natural channel at $h^+ = 2003$, included for comparison. (*d*) Premultiplied spectrum of the excess streamwise velocity, in local friction scaling, $k_x(E^*_{uu,C92} - E^*_{uu,C90})$. Contours are −0.05(0.05)0.5. The thicker contour is $\Delta E_{uu} = 0$, and the dashed one is negative. The dashed diagonal in (*a*,*b*,*d*) is $\lambda_x = 9y$. (*e*) Mean-squared intensity of the large-scale streamwise-velocity fluctuations for wavelengths $\lambda_x \geqslant 2h$ and $\lambda_z \geqslant h$, in local friction scaling. Symbols as in table 1. (*f*) As in (*e*) but normalized with the local friction velocity measured at $y/h = 0.4$.

of the energy, but fails in the large-scale inactive wedge, where the IRANS normalized spectrum exceeds the natural one.

That this is due to the scaling of the inactive motions with the stress of the outer fluctuations is tested in figure 6(*e*,*f*), which presents the behaviour of the large-scale velocity fluctuations near the wall. Those streamwise fluctuations have been filtered to include only wavelengths longer and wider than $\lambda_x = 2h$ and $\lambda_z = h$, and are only plotted below $y^+ = 100$. The figures therefore only include contributions from the inactive wedge. In figure 6(*e*) they are scaled with their local u_*, and the collapse is poor. Inspection of figure 6(*b*) suggests that the active cores of structures with those wavelengths are located at $y/h \approx 0.4$–0.5, whose stresses would provide their velocity scales. Figure 6(*f*) includes the same data as figure 6(*e*), but scaled with $u_*(0.4h)$. The scaling is much better, and the same is true when u_* is taken at $y = 0.5h$. Note that the almost discontinuous stress jump in the blended case B9L, which lies between the intensities in the figure and their assumed scaling velocities, constitutes a particularly stringent test for the non-local scaling of the inactive motions.

Bradshaw (1967) used a similar technique to test the influence of the intensity of the outer velocity fluctuations on the near-wall inactive motions, modifying the outer shear of his boundary layer by means of a pressure gradient.

3.2. *Energy balance*

The plateau of c_{uv} over $y/h \approx 0.1$–0.6 is usually associated with the equilibrium logarithmic layer. We saw in the previous section that the part of the classical theory linking the velocity fluctuations with the tangential Reynolds stress holds in the IRANS simulations. On the other hand, the argument stating that the mean profile adjusts itself so that the production of turbulent energy, $\Pi = -\langle uv\rangle \partial_y U$, balances the dissipation, ϵ does not hold. Figure 7(*a*–*c*) shows the production, the dissipation, and the ratio Π/ϵ. In the natural case, production exceeds dissipation in the buffer layer, and both are roughly in equilibrium across the logarithmic layer. Above $y \approx 0.5h$, the production decreases as both $\langle uv\rangle$ and the mean shear approach zero at the centreline, while the dissipation does not vanish. The resulting energy deficit is compensated by the gradient of a turbulent diffusion flux, $\partial_y\langle vK\rangle$, where K is the kinetic energy, whose ultimate source is the production excess near the wall (figure 7*d*). Other contributions, such as the pressure and viscous diffusion terms, are negligible except very close to the wall (Mansour, Kim & Moin 1988; Hoyas & Jiménez 2008; Tuerke 2011).

Figure 7(*a*–*c*) shows that the same general balance applies to the IRANS simulations C91 and C92, although the details are different. The production and the dissipation follow trends similar to the intensities; both are stronger where the shear is higher than normal, and lower where it is weaker, but those changes do not cancel each other everywhere. The ratio Π/ϵ in figure 7(*c*) deviates more from equilibrium in the IRANS simulations than in the natural one, specially below $y \approx 0.3h$ and in the blended case. The turbulent diffusion fluxes change to compensate the imbalance (figure 7*d*), to the point that their gradients occasionally switch sign with respect to their natural values. The overall flux, $\langle vK\rangle$, remains positive in all our simulations.

The importance of the advective energy fluxes argues against local equilibrium models, which was one of the questions posed in the introduction, and supports a more distributed view of the energy balance. For example, the ratio $L_{adv} = \langle vK\rangle/\epsilon$ is a 'diffusion length' representative of the thickness of the layer whose dissipation could be fully accounted for by the advective energy flux, and figure 7(*e*) shows that L_{adv} is of the order of or larger than y across the equilibrium layer. The implication is that the energy of the turbulent structures does not dissipate locally, but is advected over

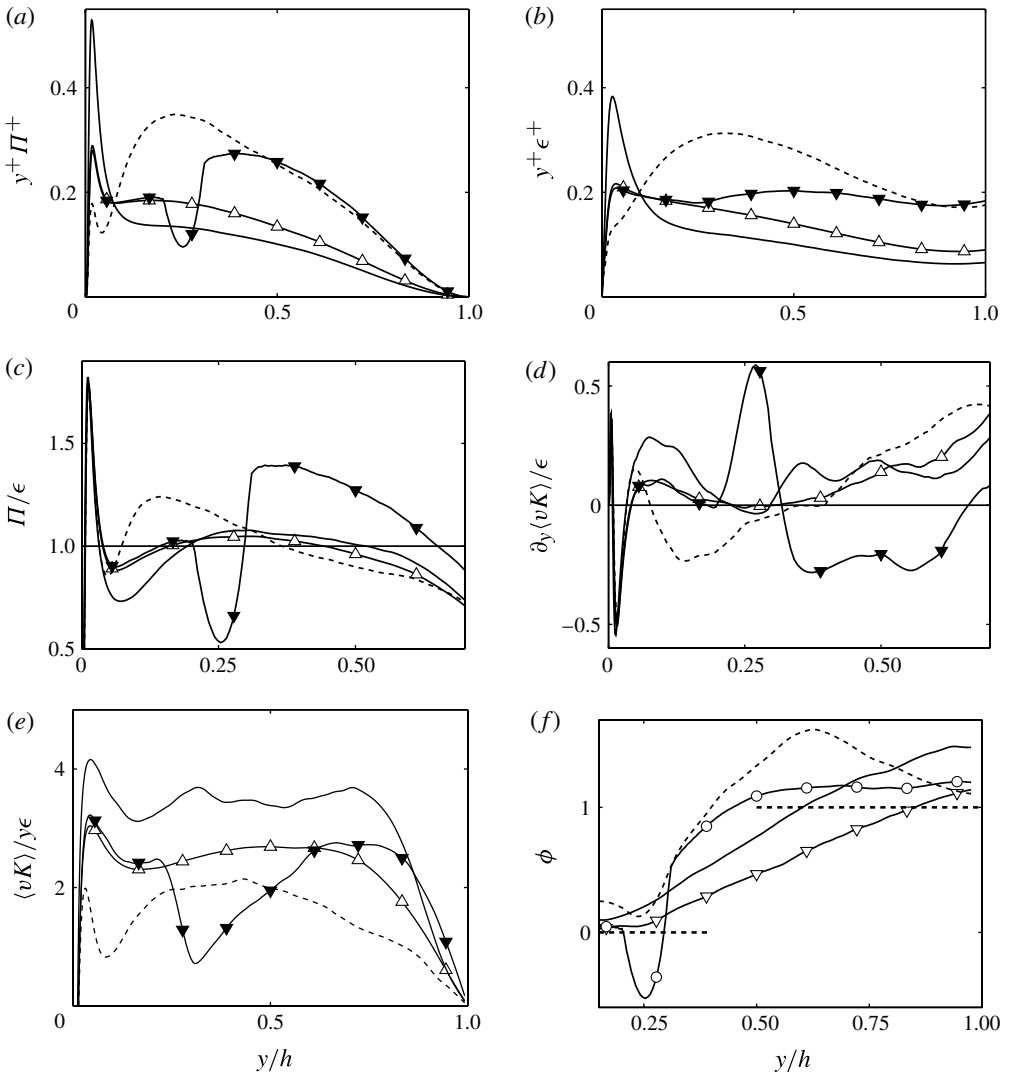

FIGURE 7. (*a*) Compensated turbulent energy production. (*b*) Compensated dissipation. (*c*) Ratio of the turbulent kinetic energy production to the dissipation. (*d*) Turbulent transport contribution to the energy budget. (*e*) Turbulent diffusion energy length. Symbols in (*a–e*) as in table 1. (*f*) Transition in the blended case B9L, from the natural profile C90 below the blend, to C92 above it, in terms of the fractional coefficient defined in (3.5). –○–, kinetic energy production; – – –, streamwise fluctuations, u'^2; ——, transverse fluctuations, $v'^2 + w'^2$; –▽–, dissipation. The dashed horizontal lines are $\phi = 0$, C90 and $\phi = 1$, C92.

layers of the order of their distance to the wall before equilibrating. That advection is what appears as a turbulent diffusion flux. It was shown by Flores & Jiménez (2010) that individual eddies, marked in their case by a particularly strong tangential stress, move towards and away from the wall with wall-normal advection velocities of the order of u_τ, which agrees with the observed values of v', and, since the plane-averaged wall-normal velocity $\widehat{v}_{00}$ vanishes at all times, the flux $\langle vK\rangle$ is a weighted average of the energy being advected upwards and downwards. The positive fluxes in figure 7(*e*)

imply that the eddies moving away from the wall are stronger on average than those moving towards it, which is consistent with the shape of the intensity profiles. In natural channels such processes are difficult to disentangle because all eddies share a common velocity scale, but IRANS simulations provide a way of manipulating the fluxes by imposing different velocity scales at different wall distances.

The blended IRANS simulation B9L was undertaken for that purpose. As described in § 2, it is constructed from the natural profile C90 near the wall and the rounded one C92 above the blend, with a sharp increase in the shear across the blending layer. Its energy budget near the wall is essentially normal, presumably because the time scales in the vicinity of the buffer layer are fast enough to equilibrate the flow. Above the 'discontinuity', both the production and the dissipation increase, but it is interesting that, while the production in figure 7(*a*) adapts almost immediately to that of C92, the change of the dissipation in figure 7(*b*) is more gradual. In particular, note that the dissipation profile does not show any trace of the dip in the energy production within the blending layer. As a result of those different adaptation rates, the ratio Π/ϵ increases sharply above the blend (figure 7*c*), and the diffusion fluxes in figure 7(*d*) change accordingly.

Figure 7(*f*) compares the different relaxation rates by means of the ratio

$$\phi_\xi = \frac{\xi^+_{B9L} - \xi^+_{C90}}{\xi^+_{C92} - \xi^+_{C90}}, \tag{3.5}$$

which is plotted for different (ξ) quantities, and which changes from $\phi = 0$ for C90 to $\phi = 1$ for C92. It is difficult not to interpret that plot as an evolution from left to right. The generation and transfer of turbulent energy in parallel shear flows starts with the tangential Reynolds stress, which feeds energy into the streamwise velocity component, from where it is redistributed by pressure to the transverse velocities, and finally to viscous dissipation across the inertial energy cascade (Pope 2000, pp. 315–317). Each of those steps takes a fraction of an eddy-turnover time (Kolmogorov 1941; Kerr 1990), which is $O(y/u_\tau)$ in wall turbulence.

The simplest interpretation of figure 7(*f*) is that, as the eddies move across the blend into the region of stronger shear, their energy production rate and streamwise velocity fluctuations, u'^2, increase almost immediately. After a lag, which can be estimated from the figure as $\Delta y \approx y/3$, the transverse components, $v'^2 + w'^2$, begin to receive energy and grow, and it is only after a further lag of the same magnitude that the dissipation begins to adjust. Note that the velocities, which start to receive energy before the dissipation has been fully established, overshoot their asymptotic values, and only decay towards it after the viscous dissipation has had time to act. That is especially clear in u'^2, while the transverse velocities never have time to start decaying in this particular simulation. Note that the spatial offsets just mentioned are consistent with temporal lags of the order of an eddy turnover with an advection velocity of the order of u_τ, as discussed above. Note also that an alternative interpretation emphasizing the advection of fluid particles instead of coherent eddies would result in essentially the same observations. In that sense, the two interpretations could be considered equivalent, although the long relaxation lengths in figure 7(*f*) probably require that the energy of the particles stays 'unmixed' for some time.

4. Conclusions

We have shown that simulations of plane turbulent channels with prescribed mean velocity profiles can be used to study the physics of turbulent fluctuations above the

buffer layer. In the first place, we have shown that fixing the mean velocity to its correct value does not change the magnitude of the velocity fluctuations, while even slightly incorrect profiles have a large effect on the intensities, following the local mean shear rather than the mean velocity. Fixing the velocity profile is equivalent to applying a volumetric force, uniform over wall-parallel planes, but with relatively strong temporal fluctuations. Only the temporally averaged force appears to matter, and a simulation in which the fixed velocity profile was substituted by an equivalent fixed force gave similar results. We have interpreted those results as disproving models, such as the one discussed in the introduction, in which the feedback of the fluctuations on the mean profile, or more generally of the velocity profile averaged over relatively large regions, is essential to the stability of the equilibrium of the flow.

Nevertheless, the most interesting results refer to the dynamics of the smaller eddies, rather than to the mean velocity profile. The equilibrium of the latter requires the interplay of relatively weak forces, such as the mean viscous force or the Reynolds stresses, and evolves over correspondingly slow time scales. In most of the present experiments, the mean profile is simply fixed. The fluctuations have faster time scales, and respond to stronger local forces, mainly pressure. Consider an eddy, defined in the sense of Obukhov (1941) as a fluid parcel of characteristic size λ and internal velocity differences u_λ, which stays identifiable over a turnover time of order λ/u_λ. It undergoes accelerations of order $\boldsymbol{u}\nabla\boldsymbol{u} \sim u_\lambda^2/\lambda$, implying forces per unit mass of the same magnitude. Assuming inertial scaling, $u_\lambda \sim (\epsilon\lambda)^{1/3} \approx u_\tau\,(\lambda/y)^{1/3}$, the implied forces are of order $u_\tau^2\,(y^2\lambda)^{-1/3}$, and are stronger than the Reynolds stress gradient, $O(u_\tau^2/h)$, as long as $\lambda/y < (h/y)^3$. A similar argument shows that the eddy forces are stronger than the mean viscous force, $\nu\partial_y U \sim \nu u_\tau/y^2$, if $\lambda/y < y^{+3}$. Both are easily satisfied for all reasonably isotropic scales in the overlap region, for which $\lambda \lesssim y$. That is probably the reason why we find that the details of how the mean profile is modified are irrelevant to the behaviour of the fluctuations, which only feel its effect when integrated over an eddy turnover.

The experiments in this paper have been designed to explore the internal structure of eddies, in the sense just defined, by creating profiles that interact with them differently at different heights, such as with higher shear near or far from the wall, or with sharp shear changes. That allows us to untangle internal energy-redistribution paths which are difficult to separate otherwise, without necessarily tracking the eddies individually.

Consistent with the decoupling predicted by the previous arguments, the isotropy coefficients of the eddies weakened or strengthened by the profile-fixing experiments are similar to those of natural channels above the buffer layer, even if the intensities are incorrect. In particular, the correlation coefficient between u and v changes little, and the intensity profiles collapse well when normalized with a y-dependent friction velocity that takes into account the extra stresses introduced by fixing the profile.

The correlation coefficient near the wall is lower than normal in simulations that have a higher shear in the central part of the channel, and vice versa, reflecting the effect of the inactive motions carrying energy but no tangential stresses, as originally hypothesized by Townsend (1961). In particular, we have shown that those inactive eddies are restricted to a spectral 'wedge' of large scales near the wall, whose intensities are not controlled by the local shear stress, but by the stresses in 'active' cores located farther from the wall at the same wall-parallel scales.

The production and dissipation of the kinetic energy are not in local equilibrium, with the imbalance being compensated by turbulent diffusion, suggesting that it is due to the different rates at which the various properties adjust to the shear when the fluid

is advected towards or away from the wall. Particularly instructive are simulations in which the shear increases relatively sharply above a blending layer. The tangential Reynolds stress is the fastest to respond to the higher shear, followed closely by the energy of the streamwise fluctuations, then by that of the transverse fluctuations, and finally by the dissipation, in agreement with the classical understanding of the energy transfer in shear flows. The offsets between the evolution of the different variables are of the order of the wall distance, strongly suggesting that the equilibrium between production and dissipation in the inertial region has to be understood in terms of the integrated energy over wall-attached layers, rather than locally at a single wall distance.

If the offsets are interpreted as temporal delays in the evolution of eddies advected with wall-normal velocities of the order of u_τ, as suggested both by the v' profile and by previous eddy-tracking studies (Flores & Jiménez 2010), the implied lags are of the order of the local eddy-turnover time, in agreement with the classical Kolmogorov (1941) cascade model.

Acknowledgements

This work was supported in part by the CICYT grant TRA2009-11498, by the European Research Council grant ERC-2010.AdG-20100224, and by an allocation of computer time from the Spanish Supercomputing Network. F.T. was supported by the Erasmus program. We are indebted to A. G. Gungor for many fruitful discussions.

REFERENCES

DEL ÁLAMO, J. C., JIMÉNEZ, J., ZANDONADE, P. & MOSER, R. D. 2004 Scaling of the energy spectra of turbulent channels. *J. Fluid Mech.* **500**, 135–144.

BRADSHAW, P. 1967 Inactive motions and pressure fluctuations in turbulent boundary layers. *J. Fluid Mech.* **30**, 241–258.

CESS, R. D. 1958 A survey of the literature on heat transfer in turbulent tube flow. *Report* 8-0529-R24. Westinghouse Research.

FLORES, O. & JIMÉNEZ, J. 2010 Hierarchy of minimal flow units in the logarithmic layer. *Phys. Fluids* **22**, 071704.

DEGRAAFF, D. B. & EATON, J. K. 2000 Reynolds number scaling of the flat-plate turbulent boundary layer. *J. Fluid Mech.* **422**, 319–346.

HOYAS, S. & JIMÉNEZ, J. 2006 Scaling of the velocity fluctuations in turbulent channels up to $Re_\tau = 2003$. *Phys. Fluids* **18**, 011702.

HOYAS, S. & JIMÉNEZ, J. 2008 Reynolds number effects on the Reynolds-stress budgets in turbulent channels. *Phys. Fluids* **20**, 101511.

HULTMARK, M., VALLIKIVI, M., BAILEY, S. C. C. & SMITS, A. J. 2012 Turbulent pipe flow at extreme Reynolds numbers. *Phys. Rev. Lett.* **108**, 094501.

JARRIN, N. 2007 Synthetic inflow boundary conditions for numerical simulation of turbulent flow. PhD thesis, Engineering and Phys. Sci., University of Manchester.

JIMÉNEZ, J. 1993 Energy transfer and constrained simulations in isotropic turbulence. In *CTR Annu. Res. Briefs*, pp. 171–186. Stanford University.

JIMÉNEZ, J. 2010 Wall turbulence with arbitrary mean velocity profiles. In *CTR Annu. Res. Briefs*, pp. 17–24. Stanford University.

JIMÉNEZ, J. 2012 Cascades in wall-bounded turbulence. *Annu. Rev. Fluid Mech.* **44**, 27–45.

JIMÉNEZ, J. & HOYAS, S. 2008 Turbulent fluctuations above the buffer layer of wall-bounded flows. *J. Fluid Mech.* **611**, 215–236.

JIMÉNEZ, J. & PINELLI, A. 1999 The autonomous cycle of near wall turbulence. *J. Fluid Mech.* **389**, 335–359.

KERR, R. M. 1990 Velocity, scalar and transfer spectra in numerical turbulence. *J. Fluid Mech.* **211**, 309–332.

KIM, J., MOIN, P. & MOSER, R. D. 1987 Turbulence statistics in fully developed channel flow at low Reynolds number. *J. Fluid Mech.* **177**, 133–166.

KOLMOGOROV, A. N. 1941 The local structure of turbulence in incompressible viscous fluids a very large Reynolds numbers. *Dokl. Akad. Nauk SSSR* **30**, 301–305.

MANSOUR, N. N., KIM, J. & MOIN, P. 1988 Reynolds-stress and dissipation-rate budgets in a turbulent channel flow. *J. Fluid Mech.* **194**, 15–44.

METZGER, M. M. & KLEWICKI, J. C. 2001 A comparative study of near-wall turbulence in high and low Reynolds number boundary layers. *Phys. Fluids* **13**, 692–701.

MIZUNO, Y. & JIMÉNEZ, J. 2011 Mean velocity and length scales in the overlap region of wall-bounded turbulent flows. *Phys. Fluids* **23**, 085112.

MOSER, R. D., KIM, J. & MANSOUR, N. N. 1999 Direct numerical simulation of a turbulent channel flow up to $Re_\tau = 590$. *Phys. Fluids* **11**, 943–945.

NAGIB, H. M., CHAUHAN, K. A. & MONKEWITZ, P. 2006 Approach to an asymptotic state for zero pressure gradient turbulent boundary layers. *Phil. Trans. R. Soc. Lond.* A **365**, 755–770.

OBUKHOV, A. M. 1941 On the distribution of energy in the spectrum of turbulent flow. *Dokl. Akad. Nauk SSSR* **32**, 22–24.

PERRY, A. E. & ABELL, C. J. 1975 Scaling laws for pipe-flow turbulence. *J. Fluid Mech.* **67**, 257–271.

PERRY, A. E., HENBEST, S. M. & CHONG, M. S. 1986 A theoretical and experimental study of wall turbulence. *J. Fluid Mech.* **165**, 163–199.

PERRY, A. E. & LI, J. D. 1990 Experimental support for the attached-eddy hypothesis in zero-pressure-gradient turbulent boundary layers. *J. Fluid Mech.* **218**, 405–438.

POPE, S. B. 2000 *Turbulent Flows*. Cambridge University Press.

SHE, Z.-S. & JACKSON, E. 1993 Constrained Euler system for Navier–Stokes turbulence. *Phys. Rev. Lett.* **70**, 1255–1258.

SHTILMAN, L. & CHASNOV, J. R. 1992 LES versus DNS: a comparative study. In *Proc. CTR Summer School*, pp. 137–143. Stanford University.

SIMENS, M. P., JIMÉNEZ, J., HOYAS, S. & MIZUNO, Y. 2009 A high-resolution code for turbulent boundary layers. *J. Comput. Phys.* **228**, 4218–4231.

SMITS, A. J., MACKEON, B. J. & MARUSIC, I. 2011 High-Reynolds number wall turbulence. *Annu. Rev. Fluid Mech.* **43**, 353–375.

SPALART, P. R., MOSER, R. D. & ROGERS, M. M. 1991 Spectral method for the Navier–Stokes equations with one infinite and two periodic dimensions. *J. Comput. Phys.* **96**, 297–324.

TOWNSEND, A. A. 1961 Equilibrium layers and wall turbulence. *J. Fluid Mech.* **11**, 97–120.

TOWNSEND, A. A. 1976 *The Structure of Turbulent Shear Flow*, 2nd edn. Cambridge University Press.

TUERKE, F. 2011 An inverse RANS simulation of a turbulent channel flow at moderate Reynolds numbers. Master thesis, Universidad Politécnica Madrid.

ZHOU, Y. 1993 Interacting scales and energy transfer in isotropic turbulence. *Phys. Fluids* **A 5**, 2511–2524.